Dopamine synchronizes hippocampal-prefrontal networks

Benedito A de Oliveira-Junior[1], Fernando E Padovan-Neto[3], Nandakumar S Narayanan[4], Joao P Leite[1], Rafael N Ruggiero[1,2]

[1] Department of Neuroscience and Behavioral Sciences, Ribeirão Preto Medical School - University of São Paulo, Ribeirão Preto, SP, 14049-900, Brazil.

[2] Department of Psychobiology, Escola Paulista de Medicina - Universidade Federal de São Paulo, São Paulo, SP, 04024-002, Brazil.

[3] Department of Psychology, Faculty of Philosophy, Sciences and Letters of Ribeirão Preto - University of São Paulo, Ribeirão Preto, SP, 14040-901, Brazil.

[4] Department of Neurology, University of Iowa, Iowa City, IA, 52242, USA.

Correspondence: benedito.oliveira@usp.br, rnruggiero@unifesp.br

Abstract

Interactions among brain networks support cognition and behavior. Oscillatory activity may contribute to this process by coordinating distant neuronal populations. A crucial step toward elucidating brain function and its emergent properties is understanding the mechanisms that dynamically modulate functional connectivity in response to environmental challenges and physiological demands. Dopamine (DA) is well-positioned to modulate this process, given its role in altering neuronal excitability and regulating oscillatory cognitive networks, such as the hippocampus-prefrontal cortex (HPC-PFC) networks. However, it is mostly unknown how dopamine modulates

HPC-PFC synchrony. Here, we recorded HPC and PFC activity in rats while manipulating dopamine levels. Our results show that dopamine dose-dependently induces HPC-PFC theta synchrony. This effect was not reproduced by selective activation of D_1-like (SKF-38393) or D_2-like (quinpirole) receptors, nor by the D_1/D_2 non-selective agonist apomorphine. Thus, dopamine's modulatory effects on HPC-PFC activity may depend on the precise interplay between dopamine receptor subtypes. Our findings provide evidence that dopaminergic neurotransmission plays a central role in regulating HPC-PFC oscillatory dynamics, specifically promoting synchronization in slow-frequency oscillations.

Keywords: Dopamine, functional connectivity, hippocampal-prefrontal cortex, phase synchrony, theta oscillations.

Introduction

Brain activity underlying behavior is highly flexible and emerges from the coordinated dynamics of distributed neuronal networks. Neural oscillations are believed to promote the formation of neuronal ensembles and facilitate communication between ensembles from distinct brain regions (Fries, 2005; Buzsáki, 2010). Oscillations are possibly the most energy-efficient mechanism for the temporal coordination of neural activity (Buzsáki & Draguhn, 2004). Thus, investigating how oscillatory synchrony operates is particularly interesting for understanding the dynamic coordination of brain activity.

Fries (2005; 2015) proposes that interareal coherence creates brief, milliseconds-scale windows in which inputs from one neuronal group are preferentially

transmitted and read out by another. Because coherence is flexible and state-dependent, it may be tuned by neurophysiological processes such as synaptic plasticity (Uhlhaas et al., 2010) and neuromodulation, particularly dopaminergic (Beeler & Dreyer, 2019), thereby enabling selective, dynamic routing of information across brain networks.

Dopamine (DA), acting through D_1- and D_2-like receptors, powerfully influences neuronal excitability and synaptic efficacy (Goto & Grace, 2005; Lezcano & Bergson, 2002; Robinson & Sohal, 2017), which could provide the basis for DA to contribute to interareal synchronization. Specifically, the participation of DA in oscillatory synchrony has been investigated in the hippocampus-prefrontal cortex (HPC-PFC) networks, which are central to cognition and emotion and are coordinated by hippocampal theta rhythms (Benchenane et al., 2011; Ruggiero et al., 2021; Sigurdsson & Duvarci, 2016; Spellman et al., 2015). In working memory tasks, HPC-PFC theta synchrony varies dynamically and is usually correlated to individual performance (Benchenane et al., 2011; Fujisawa & Buzsáki, 2011; Sigurdsson et al., 2010; O'Neill et al., 2013). Interestingly, it is known that DA release in the cortex increases during working memory tasks (Phillips et al., 2004). Notably, Benchenane et al. (2010) showed that HPC-PFC theta coherence could be reproduced by PFC local DA administration in anesthetized rats. Furthermore, both agonism and antagonism of D_1- and D_2-like DA receptors are shown to be associated with changes in HPC-PFC theta synchrony (Xu et al., 2016; Perreault et al., 2017; Gener et al., 2019), reinforcing the DA proposal as a neural synchrony modulator (Beeler & Dreyer, 2019).

67 Together, the literature suggests that dopaminergic neurotransmission plays a
68 role in regulating HPC-PFC oscillatory activity, influencing power or coherence
69 (Benchenane et al., 2010; Xu et al., 2016; Perreault et al., 2017; Gener et al., 2019).
70 However, this process is still poorly understood. For instance, in a small sample,
71 Benchenane et al. (2010) reported that local DA administration in the PFC increased
72 theta coherence without altering theta power in either PFC or HPC. Since coherence is
73 a measure dependent on power, these findings suggest that there may also be phase
74 synchrony modulation, i.e., a power-unbiased and volume-conduction-free
75 synchronization. In this study, we tested the hypothesis that DA modulates HPC-PFC
76 oscillatory phase synchrony. Here, we investigated the impact of DA administration on
77 HPC-PFC functional connectivity, and whether these effects are reproduced by selective
78 D_1- and D_2-like DA single-receptor agonism or non-specific apomorphine (APO) agonism.
79 Our findings reveal that DA induces HPC-PFC theta phase synchrony dose-dependently,
80 and receptor agonists do not fully reproduce this effect. Therefore, our data suggest that
81 DA has an essential but complex role in regulating HPC-PFC oscillatory activity,
82 influencing not only power and coherence but also phase synchrony in theta
83 frequencies.

84

85 **Materials and Methods**

86 **Animals**

87 Forty-two male seven-week-old Sprague Dawley rats were used in this study. The
88 animals were housed in standard rodent cages and kept in a controlled-temperature
89 room (24 ± 2 ºC) that operated in cycles of 12 hours of light and 12 hours of dark, with

90 lights on at 7:00 a.m. All animals had ad libitum access to food and water. This study was
91 approved by the local ethics committee on animal experimentation (Ribeirão Preto
92 Medical School, University of São Paulo; protocol number: 74/2021).

93 **Surgery and electrode implantation**

94 Rats were anesthetized under urethane (1.2 g/Kg in NaCl 0.15 M, i.p., Sigma-
95 Aldrich) and placed in a stereotaxic frame (Kopf Instruments, EUA) equipped with a
96 heating pad (Insight, Brazil) for temperature maintenance (37 ± 0.5 °C). Once the skull
97 was exposed, burr holes were drilled, targeted at the left medial PFC (anteroposterior,
98 AP: + 3.2 mm; medial-lateral, ML: - 0.5 mm; dorsal-ventral, DV: - 2.9 mm) and the left
99 dorsal HPC (AP: - 5.0 mm, ML: - 2.7 mm, DV: - 3.1 mm) for local field potential (LFP)
100 recordings, and the right lateral ventricle (LV; AP: - 0.5 mm, ML: - 1.8 mm, DV: - 3.5 mm)
101 for cannula implantation to deliver intracerebroventricular (i.c.v.) injections (Fig. 1A).

102 A single stereotrode (two intertwined, 50-µm, Teflon-coated tungsten wires) or
103 a 64-channel acute silicon probe (E64+R-50-S4-L6-200 NT, ATLAS Neuroengineering,
104 Belgium) was implanted in the PFC, and a single stereotrode was implanted in the HPC.
105 Each stereotrode was attached to a silver wire soldered into an 8-channel connector
106 (Omnectics Connector Corporation, EUA). Silicon probes and Omnetics connectors were
107 coupled to 32-channel Intan headstage preamplifiers (Intan Technologies, EUA).

108 **Extracellular recordings**

109 The recordings were acquired using the Open Ephys acquisition system (Siegle et
110 al., 2017). For recordings with silicon probes, the following parameters were used for
111 signal acquisition: 1000x gain, 30 kHz sampling rate, 0.5-7603.8 Hz bandpass filtering.

112 For recordings with tungsten wire stereotrodes, signals were acquired with 1000x gain,
113 a 5 kHz sampling rate, and 0.1-1000 Hz bandpass filtering.

114 **Drugs and experimental design**

115 Apomorphine hydrochloride, SKF-38393 hydrochloride, and quinpirole
116 hydrochloride (Sigma-Aldrich, USA) were dissolved in sterile 0.9% NaCl. Dopamine
117 hydrochloride (Sigma-Aldrich, USA) was dissolved in 0.04 mg/mL ascorbic acid to
118 prevent oxidation. Aliquots were stored at −80 °C, and each aliquot was thawed once on
119 the day of use. The doses were as follows: apomorphine 0.75, 1.5, or 3 mg/kg (i.p.);
120 dopamine 100 or 500 nmol (i.c.v.); SKF-38393 1 or 10 µg (i.c.v.); quinpirole 1 or 10 µg
121 (i.c.v.). All drugs except apomorphine were infused at a rate of 0.5 µL/min for a total
122 volume of 1µL using a Hamilton microsyringe (10 µL) connected to polyethylene tubing
123 and a 30-gauge cannula. Each animal was given a saline injection followed by a drug
124 injection. The interval between injections was at least 60 minutes to reduce or avoid the
125 influence of the previous drug on the next injection (Fig. 1B).

126 **Brain extraction and tissue processing**

127 Rats were submitted to an electrolytic lesion to mark the electrode insertion
128 sites, then sacrificed with an additional dose of thiopental (25 mg/kg, i.p.). Brains were
129 extracted and preserved in PFA (4%) for 12 hours and then in sucrose (30%) for 72 hours.
130 Histological sections were performed in the semi-frozen brains for staining with
131 hematoxylin and eosin, and subsequent verification of the electrode insertion sites.

132 **Data analysis**

133 Signal analyses were performed using custom codes in MATLAB software
134 (Mathworks, USA). LFP signals were anti-alias filtered and downsampled to 500 Hz using

135 MATLAB's *decimate* function before spectral and connectivity analyses. LFP power and
136 interareal connectivity were analyzed for delta (0.5-3Hz) and theta (6-10 Hz) bands. This
137 theta band range was selected because it encompassed the peak of the drug-related
138 change in HPC-PFC phase synchrony and therefore best captured the interareal theta
139 effect examined in our study (Fig. 1C).

140 **Spectral power**

141 Power spectral density (PSD) was calculated using Welch's method via the Fast
142 Fourier Transform algorithm available in the MATLAB software. We used 3s time
143 windows with 50% overlap and 2^{16} FFT points. We averaged the PSD estimates across
144 trials and animals, respectively. The relative power was calculated by dividing the PSD
145 estimate by the integrated power over the frequency range of 0.5-55 Hz. Whole-
146 recording spectrograms and coherograms were computed with the Chronux toolbox
147 (Bokil et al., 2010) using a 5 s moving window advanced in 2.5 s steps, a multitaper
148 method (time-bandwidth product = 3, 5 tapers), a sampling rate of 500 Hz, and a
149 frequency range of 0.5-55 Hz.

150 **Functional connectivity**

151 Spectral coherence and debiased weighted phase lag index (dwPLI - used here to
152 evaluate oscillatory phase synchrony; Vinck et al., 2011) measures were estimated using
153 cross PSDs of HPC and PFC calculated using modified Welch's periodogram method.
154 Spectral coherence is the same as that obtained by MATLAB's mscohere function and
155 indicates how well the signals being compared match each other at each frequency.
156 dwPLI was calculated as described by Vinck et al. (2011) and quantifies the phase
157 relationship between oscillations, thereby reducing zero-lag contamination due to

158 volume conduction. For coherograms of the whole recording, we used the cohgramc
159 function from the Chronux toolbox (Bokil et al., 2010) with the multi-tapered window
160 method and the same parameters described for spectrograms (Fig. 1D).

161 **Spike sorting and single-unit analysis**

162 Spike sorting was performed using *Kilosort 2.5* (Pachitariu et al., 2021). Quality
163 control of individual units was performed manually using the *phy* interactive interface
164 (https://github.com/cortex-lab/phy/). Firing-rate and spike-LFP phase-locking analyses
165 were performed using custom MATLAB scripts. Mean firing rate was quantified for
166 baseline and post-injection epochs, and spike-LFP phase locking was estimated as the
167 phase-locking value between PFC spike times and the phase of the simultaneously
168 recorded local PFC LFP. For spike-LFP analyses, the LFP was filtered in the 4-10 Hz band
169 to provide more stable phase estimates at the single-unit level. Statistical analyses were
170 based on 4-minute windows immediately before and after injection (Fig. 1D).

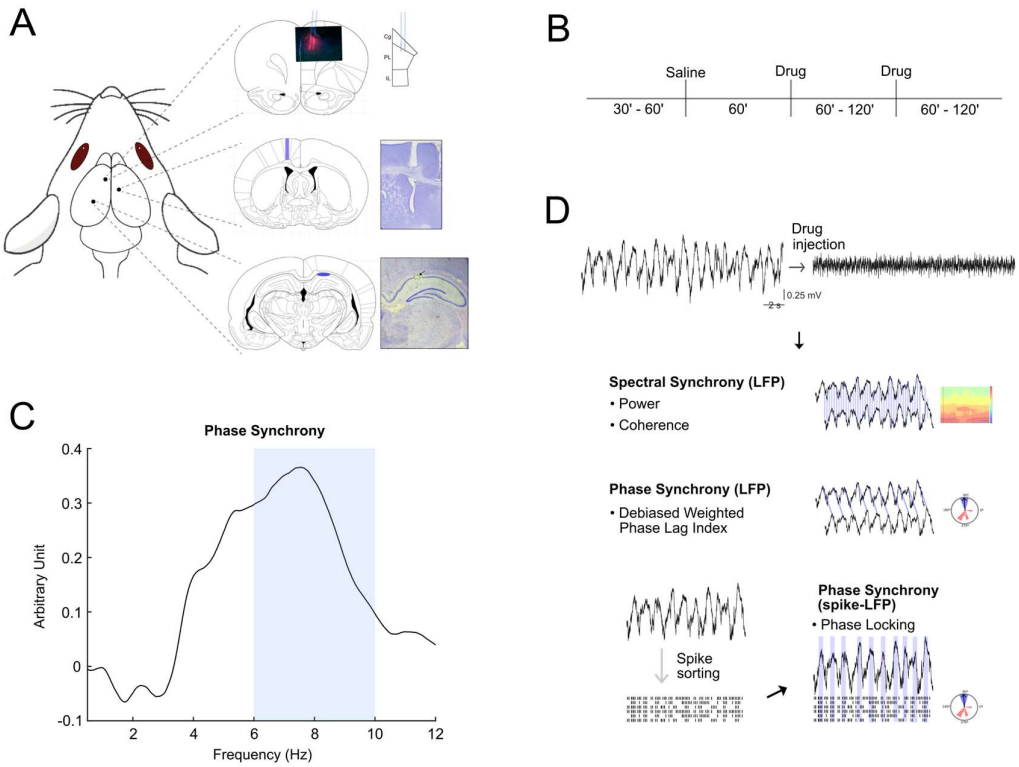

Figure 1. Experimental design and analytical workflow. (A) Surgical targeting and post hoc histology. Left: schematic showing hippocampal (HPC) and medial prefrontal cortex (PFC) recording locations from forty-two recordings, and a single intracerebroventricular (i.c.v.) cannula for drug injection. Right, top-to-bottom: representative coronal sections showing a 32-channel silicon probe spanning PFC (left hemisphere), a cannula tract into the right lateral ventricle for drug infusion, and an electrolytic lesion in CA1 (left hemisphere) marking tungsten-wire electrode placement for recordings. (B) Recording timeline. Animals underwent a 30-60 min baseline, followed by post-injection epochs (saline, then one or two drug doses; order counterbalanced). (C) The 6-10 Hz range was selected for LFP power and HPC-PFC connectivity analyses since it encompassed the peak of the post-minus-pre difference in phase synchrony (dwPLI). As dwPLI selectively captures non-zero phase-lag interactions, this approach minimizes the contribution of volume-conducted signals. (D) Analysis pipeline. Top: representative raw PFC LFP trace before and after drug infusion. Middle: spectral synchrony (power spectral density and magnitude-squared coherence) and phase-synchrony (debiased weighted phase-lag index; dwPLI) measures computed from HPC-PFC LFPs. Bottom: spike sorting followed by spike-LFP synchrony (phase locking) analysis.

Statistical analysis

We used the Shapiro-Wilk normality test to verify the data distribution. To compare two experimental groups or two conditions, we used the paired or unpaired two-tailed Student's t-test, or the non-parametric Wilcoxon matched-pairs signed-rank test using the GraphPad Prism 9.0 software (GraphPad Software, EUA).

All effects were tested using linear mixed-effects models (LMM). For DA, we fitted an LMM including the fixed factors Condition (Sal vs. DA) and DoseGroup (100 vs. 500 nmol), with a random intercept for each subject (animal nested within dose). For APO, SKF, and QUIN, we modeled Dose (saline plus the respective drug dose) as a fixed factor, with random intercepts for animal and, when applicable, an additional random intercept for injection order. Post hoc comparisons were conducted using estimated marginal means (EMMs) with a Holm adjustment for multiple comparisons. The models were implemented in R (v4.5.2; R Core Team, 2025) and run in Google Colab (Google, n.d.), a hosted Jupyter notebook environment (Kluyver et al., 2016).

Data and Code Availability

Electrophysiological data recorded for this study are publicly available at https://dandiarchive.org/dandiset/001704/draft. The code for the analysis and figure generation is accessible at https://github.com/oliveirajun/Oliveira-Junior_2026_DA.

Results

DA increases HPC-PFC theta functional connectivity and PFC spike-LFP synchrony.

We first investigated the effects of dopamine administration on HPC-PFC functional activity. Relative to baseline, i.c.v. injection of 100 nmol of DA did not induce

reliable changes of theta relative power (Fig. 2A), although the PFC theta/delta relative power ratio shows theta predominance after the drug injection (Fig. 2C). At 500 nmol, DA induced a general increase in theta relative power (PFC: theta, $t_{(12)}$=2.8, p=0.01; HPC: theta, $t_{(12)}$=2.7, p=0.02; n_{rats}=13; Fig. 2B). Consistent with these statistics, the linear mixed model reveals a significant main effect for theta power in both PFC and HPC (DA vs. Sal - PFC: $F_{(1,\ 21)}$=8.97, p<0.01; HPC: $F_{(1,\ 42)}$=5.96, p=0.02, n_{rats}=13; Fig 2D) for the highest dose (DA 500 nmol Holm-adjusted: PFC, p<0.01; HPC, p=0.01).

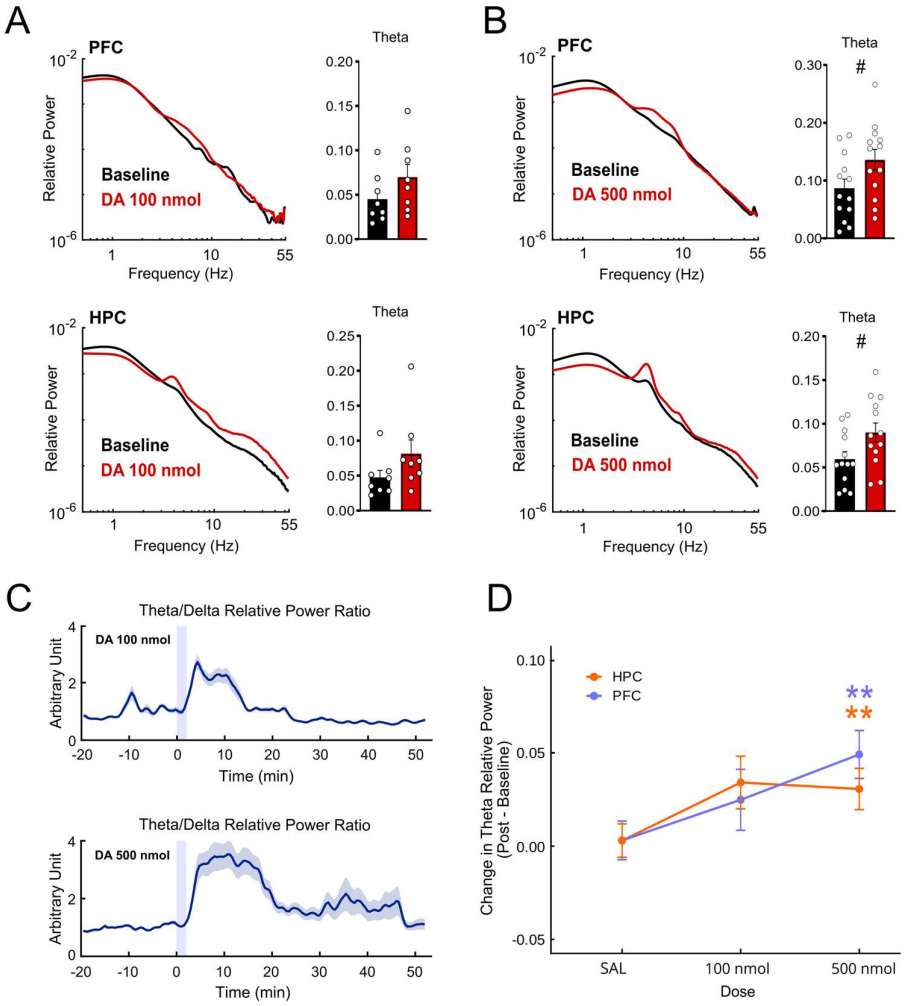

Figure 2. Dopamine (DA) increases theta relative power in PFC and HPC in a dose-dependent manner. (A-B) Log-log power spectra (10-min post-injection vs. baseline) for PFC (top) and HPC (bottom) after DA

100 nmol (A) and 500 nmol (B). Bar plots show the integrated relative power in the theta band (6-10 Hz). DA 500 nmol increased theta power in both regions (n_{rats}=13), with smaller, nonsignificant trends at 100 nmol (n_{rats}=8); paired two-tailed t-test; error bars represent SEM; (C) Time course of PFC theta/delta relative power ratio (normalized to baseline; shaded bands represent SEM; vertical shaded bar represents Injection window). DA induces an early increase in the theta/delta relative power, which is prolonged at the highest dose. (D) Dose-response of the change in theta relative power (post - baseline) for PFC and HPC. Points and error bars are linear mixed model (LMM) estimated marginal means ± SEM. # $p<0.05$ for t-tests; * $p<0.05$ for LMM main effect; ** $p<0.05$ for LMM Holm-adjusted post hoc pairwise comparison.

Similarly, interareal synchrony effects were more pronounced following the highest DA dose. While DA 100 nmol did not change the HPC-PFC oscillatory synchrony (Fig. 3A, C), DA 500 nmol reliably increased coherence at theta ($t_{(12)}$=2.7, p=0.02, n_{rats}=13; Fig. 3B, top), as well as phase synchrony (dwPLI; theta, $t_{(12)}$=3.8, $p<0.01$, n_{rats}=13; Fig. 3B, bottom). This effect was also observed when comparing the effects of DA 500 nmol with saline on theta coherence (DA vs. Sal - main effect: $F_{(1, 21)}$=4.9, p=0.04) and theta phase synchrony (DA vs. Sal: $F_{(1, 21)}$=16.28, $p<0.001$; DA 500 nmol Holm-adjusted: coherence, p=0.02; phase synchrony, $p<0.001$; Fig. 3E). Accordingly, DA 500 nmol showed a significantly stronger theta modulation compared to DA 100 nmol ($F_{(1, 21)}$=4.62, p=0.04). The dose-response curve illustrates this difference, highlighting the stronger modulation of phase synchrony, while showing a smaller overall dose effect over coherence (Fig. 3E).

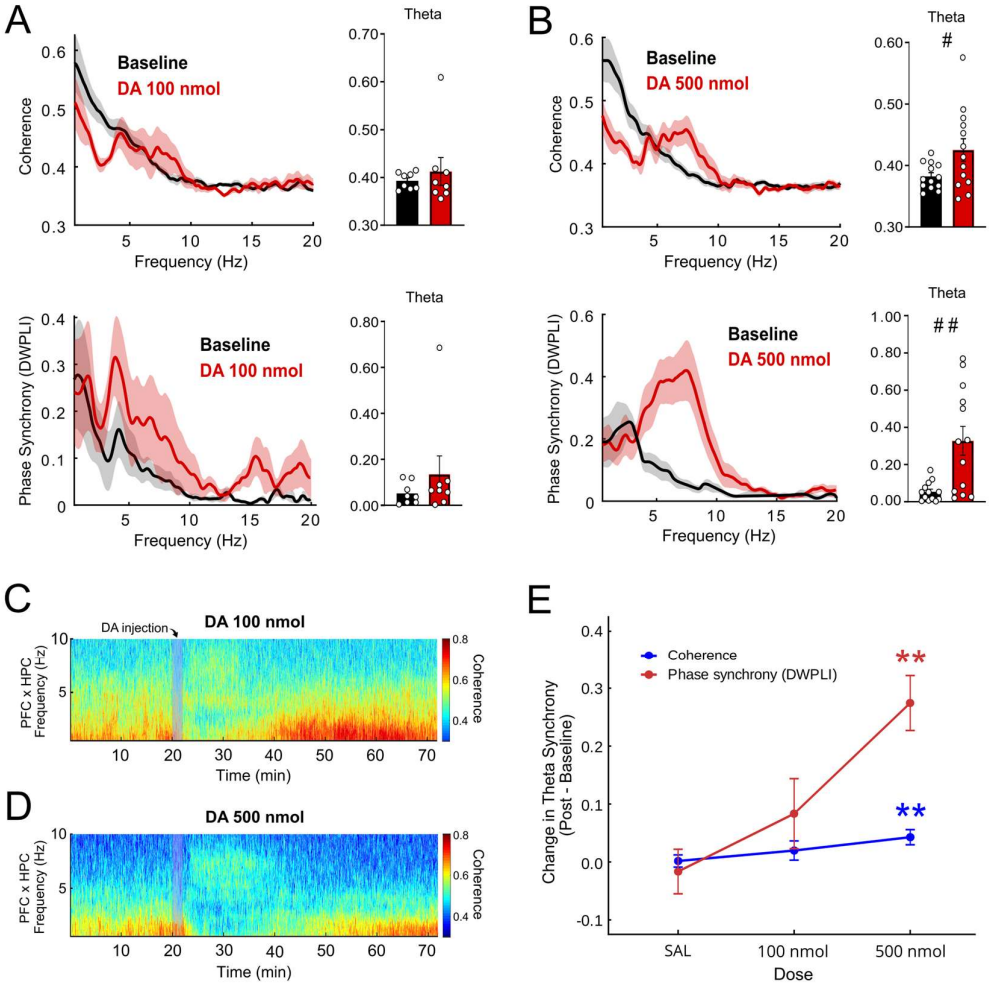

238

239 **Figure 3. DA induces HPC-PFC theta phase synchrony and coherence in a dose-dependent manner.** (A-
240 B) Spectral coherence (top) and phase synchrony by debiased weighted phase-lag index (dwPLI; bottom)
241 averaged over 10-min post-injection vs. baseline after DA 100 nmol (A) and 500 nmol (B). DA 500 nmol
242 induces theta coherence and phase synchrony (n_{rats}=13), while DA 100 nmol showed weaker increases
243 (n_{rats}=8); paired two-tailed t-tests. Error bars represent SEM. (C-D) HPC-PFC coherograms for each dose.
244 The vertical bar represents the 2-minute injection period. (E) Dose-response of change in theta synchrony.
245 DA 500 nmol shows higher theta coherence and phase synchrony modulation compared to DA 100 nmol
246 and saline. Points and error bars are linear mixed model (LMM) estimated marginal means ± SEM. #
247 $p<0.05$ and ## $p<0.01$ for t-tests statistics; ** $p<0.05$ for LMM Holm-adjusted post hoc pairwise
248 comparison.

249 To evaluate whether the DA modulatory effect is reflected in the dynamics
250 between neuronal and oscillatory activities in the PFC, we examined the phase locking
251 of PFC single-unit activity to local theta oscillations after DA 500 nmol administration.
252 DA induced a reduction in firing rate ($t_{(130)}$=2.73, $p<0.01$, $n_{neurons}$=131, n_{rats}=6; Fig. 4A).
253 Phase locking analysis revealed an increase in spike-LFP synchrony ($t_{(48)}$=-2.47, p=0.02,
254 $n_{neurons}$=49, n_{rats}=6; Fig. 4B, right) together with a change in the preferred firing phase
255 relative to theta cycles (Fig. 4B, left), which did not occur after saline injection (Fig. 4C-
256 D). These data are consistent with reports that DA receptor-dependent 4 Hz oscillations
257 in PFC exhibit strong spike-field coherence and depend on intact dopaminergic signaling
258 (Parker et al., 2014; 2017; Young-Kim et al., 2017; 2019). Together, LFP and spike-LFP
259 results indicate that DA modulates the dynamics of HPC-PFC activity dose-dependently,
260 altering the preferential phase of neuronal firing and inducing spike-LFP theta synchrony
261 in the PFC, resulting in increased functional connectivity in the pathway, particularly at
262 the highest dose applied.

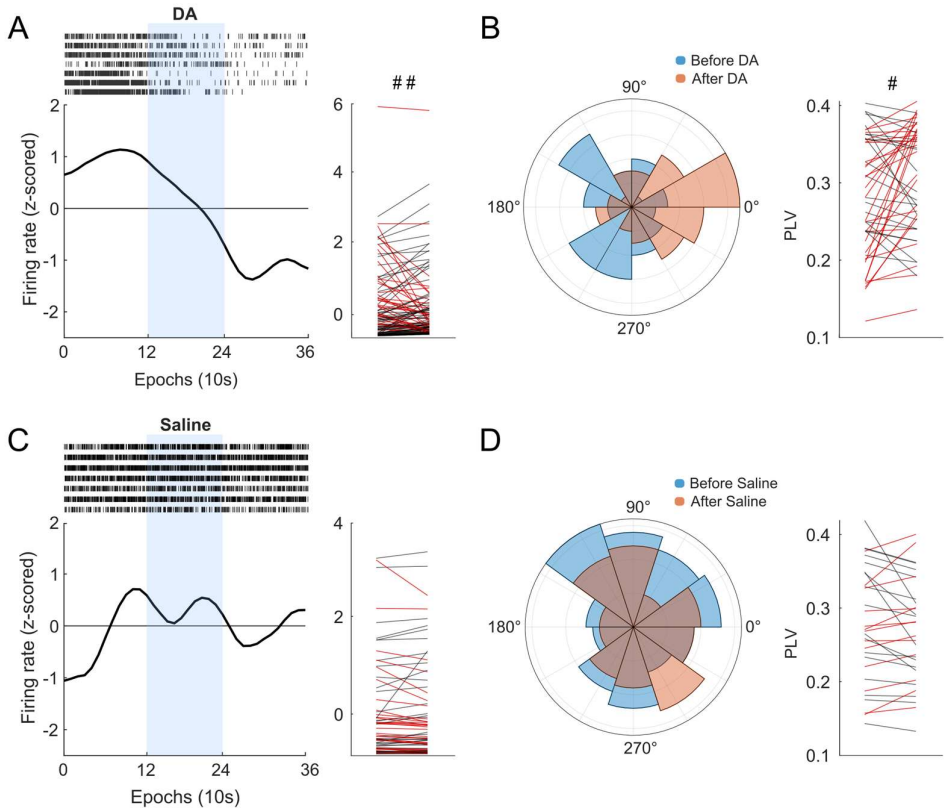

Figure 4. DA reorganizes PFC single-unit activity and enhances spike-LFP theta phase locking. (A) DA 500 nmol reduces PFC neuronal firing rates. Spike raster (top) displays spikes from representative neurons. Population z-scored firing-rate histogram shows the average decrease in neuronal activity after DA injection ($n_{neurons}$=131, n_{rats}=6). The vertical blue shaded bar represents the drug injection window. The slope graph (right) shows per-unit paired firing-rate changes; units with decreasing firing rate were highlighted in red. (B) Preferred theta phase (left) and phase locking values (right) before vs. after DA. DA 500 nmol induces spike-LFP theta synchrony and phase shift. The slope graph (right) shows per-unit paired phase locking values changes; units with increasing phase locking values were highlighted in red. (C-D) Saline condition shows no significant change ($n_{neurons}$=70, n_{rats}=6). # $p<0.05$ and ## $p<0.01$ for paired two-tailed t-tests.

274 **DA agonists SKF (D_1) and QUIN (D_2) do not reproduce DA-induced effects on HPC-PFC**
275 **oscillatory dynamics.**

276 We next tested whether selective activation of D1- or D2-like receptors could
277 reproduce the DA effects on HPC-PFC oscillatory activity at multiple doses. At theta
278 frequencies, the selective D1 agonist SKF-38393 (1 or 10 µg) was able to modulate
279 coherence (SKF vs. Sal - main effect: $F_{(2, 20)}$=4.64, p=0.02, n_{rats}=7; Fig. 5A, B, right), but
280 not phase synchrony. However, this effect did not remain significant after adjustment
281 (Holm-adjusted: p>0.05), suggesting that any differences were inconsistent across doses
282 and not reliably different from saline. Overall, SKF was associated with non-significant
283 modulation of theta relative power and HPC-PFC theta synchrony.

284 The selective D2 agonist quinpirole (QUIN, 1 or 10 µg) similarly failed to induce
285 reliable changes in HPC-PFC oscillatory activity. No consistent impact on theta relative
286 power and on interareal synchrony measures was found, indicating no reliable effects
287 produced by QUIN (Fig. 5C, D).

288 In contrast to DA, which increased theta power and HPC-PFC synchrony, isolated
289 stimulation of D_1 or D_2 did not amplify theta relative power or strengthen interareal
290 synchrony. This may indicate that concurrent D_1/D_2 activation is required to reproduce
291 the DA-induced effects.

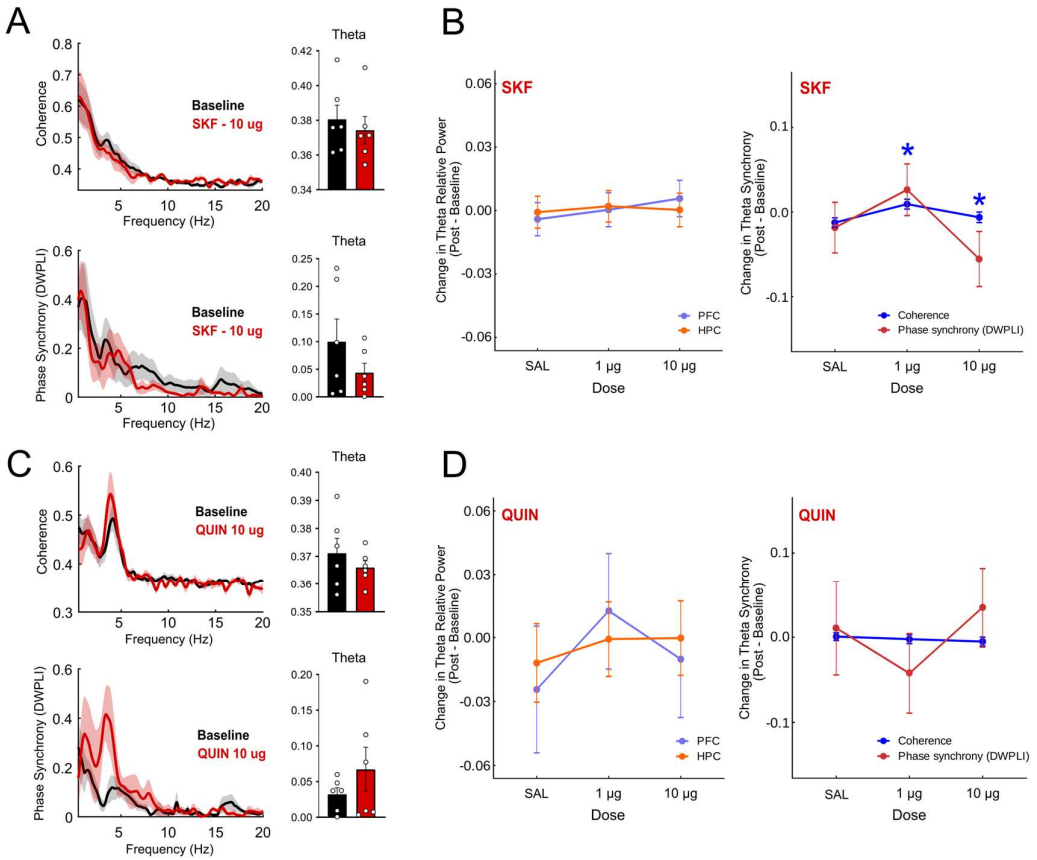

Figure 5. Selective D1 (SKF-38393) or D2 (quinpirole) receptor agonism does not reproduce DA-induced HPC-PFC theta modulation. (A) HPC-PFC coherence (top) and phase synchrony (dwPLI; bottom) averaged over 10-min post-injection vs. baseline, with theta bar plots (right; error bars represent SEM), for SKF 10 µg (n_{rats}=7). (B) Dose-response of changes in theta relative power (left) and synchrony (right; coherence, dwPLI) across saline and both SKF doses (1 µg and 10 µg). (C) Coherence and phase synchrony for QUIN 10 µg with corresponding bar plots (n_{rats}=6). Neither agonist produced consistent changes in theta power or synchrony; paired two-tailed t-tests. (D) Dose-response of power and synchrony across saline, and both QUIN doses (1 µg and 10 µg). For dose-response panels, points and error bars are linear mixed models (LMM) estimated marginal means ± SEM. * $p<0.05$ for LMM main effect.

Apomorphine exhibits a linear modulation of HPC-PFC oscillatory dynamics.

To further investigate whether DA-induced effects can be reproduced by concurrent D1/D2 activation, we administered three different doses of the non-selective DA receptor agonist apomorphine (APO; 0.75, 1.5, and 3 mg/kg; i.p.). Due to APO

306 systemic administration, analyses were conducted by contrasting the 30-40 min post-
307 injection window with the injection baseline.

308 We found that APO affects HPC-PFC oscillatory activity in a dose-dependent
309 manner. In fact, there was a main effect for theta power reduction on PFC (APO vs. Sal -
310 main effect: $F_{(3, 22)}$=3.76, p=0.03, n_{rats}=7), but not HPC (Fig. 6B). However, this effect was
311 not significant after post hoc adjustment (Holm-adjusted: p>0.05). At the lowest dose
312 (0.75 mg/kg), the theta/delta relative power ratio indicated a theta-suppressing activity
313 over time (Fig. 6A). At the intermediate dose (1.5 mg/kg), the most notable change was
314 a predominance of theta activity over delta frequencies (Fig. 6A), which contrasted with
315 the APO lowest dose. At the highest dose (3 mg/kg), there was a prominent inversion in
316 the theta/delta relative power ratio compared to the lowest dose, with theta activity
317 becoming predominant over time (Fig. 6A). Measures of inter-regional synchrony reflect
318 the modulatory capacity of the APO, although the effects are not evident by comparing
319 post-drug states directly with baseline levels. (Fig. 6C).

320 APO produced a significant main effect on both coherence (APO vs. Sal: $F(_{3, \approx 16})$ =
321 4.06, p=0.03) and phase synchrony in the theta band (APO vs. Sal: $F(_{3, \approx 14})$ = 5.07, p=0.01).
322 However, post hoc analyses revealed that only phase synchrony showed significant
323 dose-dependent differences relative to saline, surviving Holm correction (0.75 mg/kg:
324 p=0.04; 1.5 mg/kg: p=0.04; 3 mg/kg: p=0.02; Fig. 6D), whereas no individual dose
325 reached statistical significance for coherence after correction. Together, these findings
326 point to a predominant influence of APO on phase synchrony over amplitude-related
327 coupling. Dose-response curves illustrate the dose-dependent action of APO, showing a

modest modulation of relative power and coherence but a strong positive modulation of phase synchrony across theta frequencies as the dose increases (Fig. 6B, D).

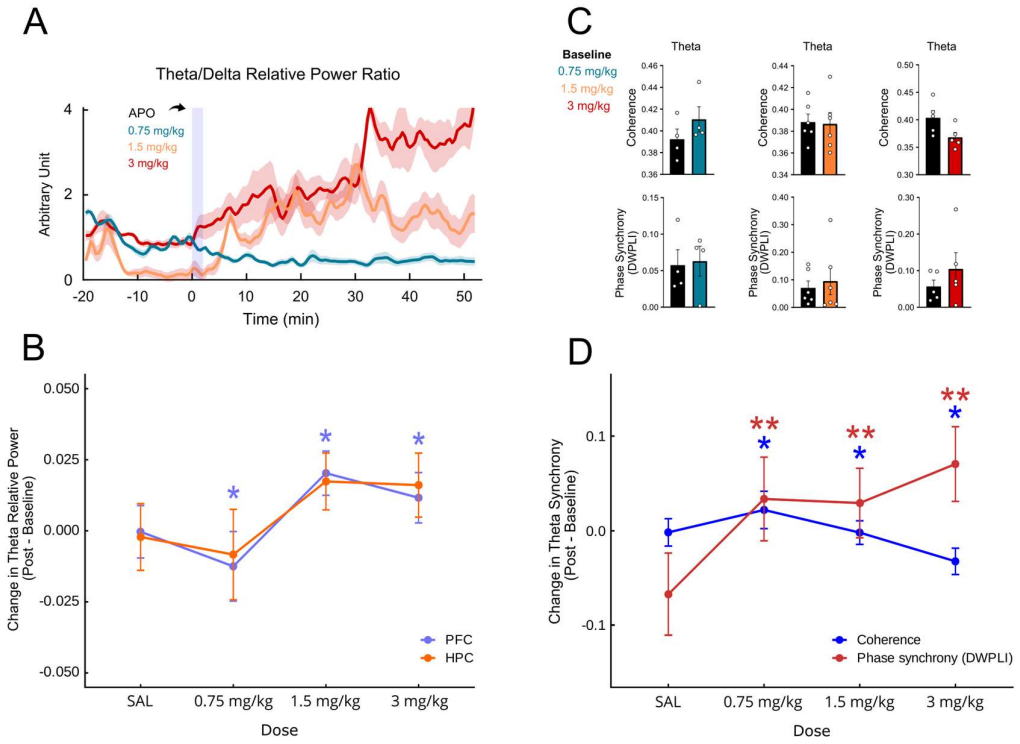

Figure 6. Apomorphine (i.p.) induces a dose-dependent modulation of HPC-PFC theta activity. (A) PFC theta/delta relative power ratio over time for 0.75, 1.5, and 3 mg/kg (normalized to baseline). Increasing the dose leads to an increase in theta relative power predominance over delta. The analysis window is 30-40 min post-dose to account for delays in the onset of effect following i.p. administration. Shaded areas around the lines represent SEM. (B) Dose-response of theta relative power change (post-injection - baseline). The magnitude of the change in relative power resembles the pattern shown by the theta/delta ratio. However, LMM analysis shows that the effect is more pronounced in the PFC. (C) Theta coherence (top row) and phase synchrony (bottom row) at each dose for post-injection vs. baseline, illustrating nonsignificant dose-linked shifts in synchrony measures when compared to baseline. Paired two-tailed t-tests. Error bars represent SEM. (D) Dose-response of theta synchrony (coherence, dwPLI). Relative to the saline injection, APO induces a strong positive modulation of theta phase synchrony while reducing theta

343 coherence as the dose increases. For dose-response panels, points and error bars are linear mixed model
344 (LMM) estimated marginal means ± SEM. For all plots, n_{rats}=4 (0.75 mg/kg); n_{rats}=6 (1.5 mg/kg); n_{rats}=5
345 (3.0 mg/kg). * $p<0.05$ for LMM main effect; ** $p<0.05$ for LMM Holm-adjusted post hoc pairwise
346 comparison.

347 **Discussion**

348 In this study, we demonstrate that DA activation modulates HPC-PFC oscillatory
349 dynamics under urethane anesthesia in a dose-dependent manner. Specifically, DA
350 increases functional theta connectivity, enhances theta phase synchrony, and shifts PFC
351 spike timing. Similarly, APO modulates the oscillatory activity. However, like the
352 selective D_1 and D_2 receptor agonists it fails to reproduce the full spectrum of DA-
353 induced effects.

354 Urethane anesthesia produces alternating activated and deactivated oscillatory
355 states, whose activity patterns are similar to those observed in natural sleep states
356 (Clement et al., 2008). During activated states, rapid low-amplitude theta oscillations
357 and HPC-to-PFC 4 Hz synchronization predominate. In deactivated states, there are high-
358 amplitude slow delta oscillations and a PFC to HPC 1 Hz synchronization predominance
359 (Ruggiero et al., 2018; Lopes-Aguiar et al., 2020). Experimental studies have shown that
360 sleep-wake cycles (Oishi & Lazarus, 2017) and urethane anesthesia are both regulated
361 by D_1- and D_2-like dopaminergic receptors (Monti & Jantos, 2008). Our results
362 demonstrate that DA and the non-specific agonist apomorphine, but not the selective
363 D_1 or D_2 agonists, elicit dose-dependent alterations in urethane-induced oscillatory
364 activity.

365 Both DA 100 nmol and 500 nmol doses induced theta oscillations predominance
366 for at least 10 continuous minutes, but DA 500 nmol effects were more pronounced,

367 showing higher and longer theta predominance. These results confirm previous studies,
368 indicating active DA participation in HPC-PFC theta modulation (Benchenane et al.,
369 2010; Ruggiero et al., 2021) and in sleep-wake-like systems (Oishi & Lazarus, 2017; Monti
370 & Jantos, 2008). Interestingly, it was shown that acute DA depletion abolishes REM
371 sleep, and REM can be recovered by D_2 receptor stimulation (Dzirasa et al., 2006).
372 However, D_2-pathway activation is necessary but not sufficient by itself to generate REM
373 sleep, and hyperdopaminergia is necessary but not sufficient to produce REM-like
374 oscillations during wake in behaving DAT-KO mice (Dzirasa et al., 2006). This result
375 indicates that the regulation of oscillatory states may also depend on the DA interaction
376 with other neurotransmitter systems, such as the cholinergic system (Lester et al., 2010;
377 Monti & Jantos, 2008). Indeed, cholinergic agonists can produce activated states, while
378 cholinergic antagonists produce prolonged deactivated states (Clement et al., 2008;
379 Ruggiero et al., 2018; Schall & Dickson, 2010). These results support the notion that
380 dopaminergic and cholinergic systems may interact in regulating urethane-induced
381 oscillatory states and the sleep-wake-like system (Dzirasa et al., 2006; Monti & Jantos,
382 2008).

383 We show that non-specific D_1/D_2 APO agonism has a dose-dependent effect on
384 HPC-PFC oscillatory dynamics. In low doses, APO is known to produce sedative effects
385 and increase the slow oscillations (Kropf & Kuschinsky, 1991; Monti & Jantos, 2008; Xu
386 et al., 2011); high doses induce the opposite effect (Monti & Jantos, 2008). Our data
387 confirm that low dose favored slower frequencies in the delta band and reduced theta
388 predominance, while high dose induced theta-dominant activity. This effect is likely
389 mediated by differential receptor mechanisms, with low doses preferentially activating
390 dopaminergic autoreceptors, inhibiting neuronal firing, and decreasing DA release,

391 whereas high doses stimulate postsynaptic receptors and enhance dopaminergic
392 signaling (Monti & Jantos, 2008; Skirboll et al., 1979). Additionally, low APO doses
393 reduce dopaminergic firing rate (Assié et al., 2009; Bunney et al., 1973a; 1973b; Mallet
394 et al., 2008; Xu et al., 2011), whereas higher doses can promote neuronal excitability
395 (Yanagihashi et al., 1991). At the highest doses, APO likely produced a
396 hyperdopaminergic state. Still, APO is reported to be D_2-biased (Dépatie & Lal, 2001),
397 which may explain its partial divergence from DA in shaping HPC-PFC oscillations in our
398 study. However, APO's behavioral impact depends on intact D1 receptors (Ralph-
399 Williams et al., 2002), highlighting that concurrent D1/D2 agonism can have effects that
400 depend on which receptors are available.

401 We found that DA induced HPC-PFC theta synchrony and a phase shift in PFC
402 neuronal activity. Consistent with this result, Benchenane et al. (2010) showed that DA
403 infused into the PFC of anesthetized rats could induce HPC-PFC theta coherence and
404 reorganize the preferred firing phase of PFC neurons relative to local theta cycles.
405 However, to investigate HPC-PFC synchrony, Benchenane et al. (2010) relied solely on
406 spectral coherence, which is biased by spectral power. The authors note that despite
407 the increase in coherence, there is no alteration in spectral power in both HPC and PFC,
408 suggesting that DA may induce phase synchrony independently of spectral power. By
409 using dwPLI, a measure that quantifies consistent delays between signals and reduces
410 zero-lag contamination due to volume conduction (Vinck et al., 2011), we showed that
411 DA induced genuine HPC-PFC theta synchrony rather than just amplifying shared
412 sources, and this effect was consistent across many animals following DA
413 administration.

414 In our study, single-activation of D_1 or D_2 receptors by respective selective
415 agonists was unable to induce significant effects. One possibility is that full dynamic
416 dopaminergic modulation of HPC-PFC oscillatory synchrony requires concurrent
417 activation of both D_1 and D_2 receptors to ensure a synergistic effect that no single-
418 receptor agonist could achieve. For instance, this activation is required by cortical D_1-D_2
419 receptor heteromers to drive specific cellular and synaptic responses (Xu & Yao, 2010;
420 Thompson et al., 2016; Perreault et al., 2014). However, the literature shows the
421 involvement of specific dopaminergic receptors in modulating HPC-PFC activity. Xu et al.
422 (2016) demonstrated in anesthetized rats that the administration of a D_1 receptor
423 antagonist could induce a reduction in HPC-PFC theta phase synchrony and theta power.
424 Additionally, systemic administration of a D_1 receptor agonist induced HPC-PFC theta
425 coherence in pharmacological animal models of schizophrenia, but not in control
426 animals (Perreault et al., 2017). In another study, a reduction in HPC-PFC theta phase
427 synchrony was observed in freely-moving animals after systemic D_2 receptor agonist or
428 antagonist infusion (Gener et al., 2019). A likely explanation for why our results diverge
429 from the literature regarding D_1 and D_2 effects is that the doses we used for selective
430 agonists were suboptimal, and could mean insufficient receptor engagement at the low
431 end, or activation of counter-regulatory mechanisms at the high end. Despite Perreault
432 et al. (2017) and Gener et al. (2019) administering comparable agonist doses, it was
433 delivered systemically, whereas we used the i.c.v. route, which may be related to the
434 divergent findings.

435 More broadly, it is known that prefrontal DA mostly exerts non-linear, inverted
436 U-shaped effects on cortical function, such that both hypo- and hyperdopaminergic
437 states are associated with impaired cognition and only an intermediate range of

438 receptor stimulation is optimal (Weber et al., 2022), highlighting the complex and dose-
439 sensitive nature of dopaminergic modulation. The complex DA receptor
440 pharmacodynamics, including differential activation of D_1 and D_2 receptors,
441 autoreceptors, and D_1-D_2 heteromers across dose ranges, further complicate the
442 interpretation of our negative findings with selective agonists. Also, a reduced sample
443 size in the agonist treatment groups may explain the lack of statistical significance, an
444 issue partially mitigated by our linear mixed-effects models, which account for repeated
445 measures and between-animal variability. Future work using broader dose-response
446 designs, receptor-specific antagonism, and cell-type or projection-specific
447 manipulations will be essential to learn how these receptor mechanisms shape HPC-PFC
448 synchrony. Importantly, our results were obtained under anesthesia, and it is known
449 that urethane anesthesia neuromodulatory tone and state transitions differ from
450 wakefulness. Thus, follow-up experiments in behaving animals are needed to generalize
451 the results found in this study, and to better understand DA's role in interareal
452 synchronization across wakefulness states.

453 Our findings link DA to long-range circuit-level communication, showing that DA
454 can rapidly increase low-frequency synchrony in crucial cognitive networks (HPC-PFC),
455 beyond simply changing local activity. In Parkinson's disease, cognitive impairment has
456 been associated with reduced midfrontal low-frequency rhythms, motivating the
457 investigation of biomarkers and stimulation-based approaches to restore coordination
458 (Singh et al., 2021; Narayanan et al., 2024). Our results suggest that DA loss may weaken
459 not only low-frequency frontal oscillations but also long-range HPC-PFC coupling needed
460 for cognitive performance. Clinically, this circuit-level interpretation aligns with the use
461 of apomorphine in patient cohorts reporting improvements in aspects of non-motor

462 symptom burden, including in patients with cognitive and neuropsychiatric dysfunctions
463 (Carbone et al., 2019). In schizophrenia, DA dysregulation and network dysconnectivity
464 are accompanied by medial frontal low-frequency deficits during cognitive timing
465 (Parker et al., 2017). Also, in an amphetamine hyperdopaminergic model, an increase in
466 timing variability and disruption of prefrontal temporal coding has been shown while
467 also reducing low-frequency oscillations (Weber et al., 2025). Together, these
468 observations support the translational idea that DA may help to regulate cognition by
469 tuning the timing of interactions across circuits, making low-frequency coupling and
470 spike timing potential targets for pharmacology and neuromodulation in DA-related
471 brain disorders.

472 **Conclusion**

473 We demonstrate that DA dose-dependently reconfigures HPC-PFC network
474 dynamics under urethane anesthesia, increasing theta power, enhancing theta phase
475 synchrony, and strengthening prefrontal spike-theta locking. In contrast, selective D_1 or
476 D_2 agonism failed to reproduce these effects, and apomorphine produced a dose-
477 dependent modulation of oscillatory dynamics. Importantly, phase-coupling analyses
478 that minimize zero-lag effects, thereby reducing volume-conduction and power-related
479 confounds, support the interpretation that the observed synchrony reflects genuine
480 interareal coupling, suggesting that DA rapidly regulates hippocampal-prefrontal
481 communication.

482

483

484

Funding

This study was supported by the Coordination for the Improvement of Higher Education Personnel (CAPES; B.A.O.J., grant 88887.469138/2019-00) and the São Paulo Research Foundation (FAPESP; R.N.R., grant 25/09433-4; J.P.L., grant 2016/17882-4).

Acknowledgments

We thank Antonio Renato Meirelles e Silva, Renata Caldo Scandiuzzi, and Daniela Ribeiro for their technical support, and Tamiris Prizon, José Luiz Liberato, and Leonardo Rakauskas Zacharias for their experimental support. The research was conceptualized by RNR and BAOJ. BAOJ conducted the experiments. BAOJ and RNR analyzed data. BAO-J, RNR, FEP-N, and NSN wrote the manuscript. RNR and JPL supervised the research.

Conflict of interest

The authors declare no competing interests.

References

Assié, M. B., Mnie-Filali, O., Ravailhe, V., Benas, C., Marien, M., Bétry, C., ... & Newman-Tancredi, A. (2009). F15063, a potential antipsychotic with dopamine D2/D3 receptor antagonist, 5-HT1A receptor agonist, and dopamine D4 receptor partial agonist properties: influence on neuronal firing and neurotransmitter release. European journal of pharmacology, 607(1-3), 74-83.

Beeler, J. A., & Dreyer, J. K. (2019). Synchronicity: the role of midbrain dopamine in whole-brain coordination. Eneuro, 6(2).

Benchenane, K., Peyrache, A., Khamassi, M., Tierney, P. L., Gioanni, Y., Battaglia, F. P., & Wiener, S. I. (2010). Coherent theta oscillations and reorganization of spike timing in the hippocampal-prefrontal network upon learning. Neuron, 66(6), 921-936.

Benchenane, K., Tiesinga, P. H., & Battaglia, F. P. (2011). Oscillations in the prefrontal cortex: a gateway to memory and attention. Current opinion in neurobiology, 21(3), 475-485.

Bokil, H., Andrews, P., Kulkarni, J. E., Mehta, S., & Mitra, P. P. (2010). Chronux: a platform for analyzing neural signals. Journal of neuroscience methods, 192(1), 146-151.

Bunney, B. S., Walters, J. R., Roth, R. H., & Aghajanian, G. K. (1973a). Dopaminergic neurons: effect of antipsychotic drugs and amphetamine on single cell activity. The Journal of pharmacology and experimental therapeutics, 185(3), 560-571.

Bunney, B. S., Aghajanian, G. K., & Roth, R. H. (1973b). Comparison of effects of L-dopa, amphetamine and apomorphine on firing rate of rat dopaminergic neurones. Nature New Biology, 245(143), 123-125.

Buzsáki, G. (2010). Neural syntax: cell assemblies, synapsembles, and readers. Neuron, 68(3), 362-385.

Buzsáki, G., & Draguhn, A. (2004). Neuronal oscillations in cortical networks. Science, 304(5679), 1926-1929.

Carbone, F., Djamshidian, A., Seppi, K., & Poewe, W. (2019). Apomorphine for Parkinson's disease: efficacy and safety of current and new formulations. CNS drugs, 33(9), 905-918.

Clement, E. A., Richard, A., Thwaites, M., Ailon, J., Peters, S., & Dickson, C. T. (2008). Cyclic and sleep-like spontaneous alternations of brain state under urethane anaesthesia. PloS one, 3(4), e2004.

Dépatie, L., & Lal, S. (2001). Apomorphine and the dopamine hypothesis of schizophrenia: a dilemma?. Journal of Psychiatry and Neuroscience, 26(3), 203.

Dzirasa, K., Ribeiro, S., Costa, R., Santos, L. M., Lin, S. C., Grosmark, A., ... & Nicolelis, M. A. (2006). Dopaminergic control of sleep–wake states. Journal of Neuroscience, 26(41), 10577-10589.

Fries, P. (2005). A mechanism for cognitive dynamics: neuronal communication through neuronal coherence. Trends in cognitive sciences, 9(10), 474-480.

Fries, P. (2015). Rhythms for cognition: communication through coherence. Neuron, 88(1), 220-235.

Fujisawa, S., & Buzsáki, G. (2011). A 4 Hz oscillation adaptively synchronizes prefrontal, ATV, and hippocampal activities. Neuron, 72(1), 153-165.

Gener, T., Campo, A. T., Alemany-González, M., Nebot, P., Delgado-Sallent, C., Chanovas, J., & Puig, M. V. (2019). Serotonin 5-HT1A, 5-HT2A and dopamine D2 receptors strongly influence prefronto-hippocampal neural networks in alert mice: Contribution to the actions of risperidone. Neuropharmacology, 158, 107743.

Google. n.d. Google Colab [Computer software]. Google Research. URL https://colab.research.google.com/ (accessed April 16, 2026).

Goto, Y., & Grace, A. A. (2005). Dopaminergic modulation of limbic and cortical drive of nucleus accumbens in goal-directed behavior. Nature neuroscience, 8(6), 805-812.

Kluyver T., Ragan-Kelley B., Pérez F., Granger B., Bussonnier M., Frederic J., Kelley K., Hamrick J., Grout J., Corlay S., Ivanov P., Avila D., Abdalla S., Willing C., Jupyter Development Team. (2016). Jupyter Notebooks – a publishing format for reproducible computational workflows. In Loizides F., Schmidt B. editors, Positioning and Power in Academic Publishing: Players, Agents and Agendas. Amsterdam (The Netherlands): IOS Press. p. 87–90. doi:10.3233/978-1-61499-649-1-87.

Kropf, W., & Kuschinsky, K. (1991). Electroencephalographic correlates of the sedative effects of dopamine agonists presumably acting on autoreceptors. Neuropharmacology, 30(9), 953-960.

558 Lester, D. B., Rogers, T. D., & Blaha, C. D. (2010). Acetylcholine–dopamine interactions in the
559 pathophysiology and treatment of CNS disorders. CNS neuroscience & therapeutics,
560 16(3), 137-162.
561 Lezcano, N., & Bergson, C. (2002). D1/D5 dopamine receptors stimulate intracellular calcium
562 release in primary cultures of neocortical and hippocampal neurons. Journal of
563 neurophysiology, 87(4), 2167-2175.
564 Lopes-Aguiar, C., Ruggiero, R. N., Rossignoli, M. T., Esteves, I. D. M., Peixoto-Santos, J. E.,
565
566 Romcy-Pereira, R. N., & Leite, J. P. (2020). Long-term potentiation prevents ketamine-
567 induced aberrant neurophysiological dynamics in the hippocampus-prefrontal cortex
568 pathway in vivo. Scientific reports, 10(1), 1-15.
569 Mallet, N., Pogosyan, A., Sharott, A., Csicsvari, J., Bolam, J. P., Brown, P., & Magill, P. J. (2008).
570 Disrupted dopamine transmission and the emergence of exaggerated beta oscillations
571 in subthalamic nucleus and cerebral cortex. Journal of Neuroscience, 28(18), 4795-
572 4806.
573 Weber, M. A., Sivakumar, K., Kirkpatrick, B. Q., Stutt, H. R., Tabakovic, E. E., Bova, A. S., ... &
574 Narayanan, N. S. (2025). Amphetamine increases timing variability by degrading
575 prefrontal temporal encoding. Neuropharmacology, 110486.
576 Monti, J. M., & Jantos, H. (2008). The roles of dopamine and serotonin, and of their receptors,
577 in regulating sleep and waking. Progress in brain research, 172, 625-646.
578 Narayanan, N. S., Jourahmad, Z., Cole, R. C., & Cavanagh, J. F. (2024). Cognition falters at~ 4 Hz
579 in Parkinson's disease. Trends in cognitive sciences, 28(9), 789-791.
580 O'Neill, P. K., Gordon, J. A., & Sigurdsson, T. (2013). Theta oscillations in the medial prefrontal
581 cortex are modulated by spatial working memory and synchronize with the
582 hippocampus through its ventral subregion. Journal of Neuroscience, 33(35), 14211-
583 14224.

Oishi, Y., & Lazarus, M. (2017). The control of sleep and wakefulness by mesolimbic dopamine systems. Neuroscience research, 118, 66-73.

Pachitariu, M., Rossant, C., Steinmetz, N., Colonell, J., Gopnik Bondy, A., Winter, O., ... & Beau, M. (2021). MouseLand/Kilosort: Kilosort 2.5. [computer software]. Zenodo. doi:10.5281/zenodo.4482749.

Parker, K. L., Chen, K. H., Kingyon, J. R., Cavanagh, J. F., & Narayanan, N. S. (2014). D1-dependent 4 Hz oscillations and ramping activity in rodent medial frontal cortex during interval timing. Journal of Neuroscience, 34(50), 16774-16783.

Parker, K. L., Kim, Y. C., Kelley, R. M., Nessler, A. J., Chen, K. H., Muller-Ewald, V. A., ... & Narayanan, N. S. (2017). Delta-frequency stimulation of cerebellar projections can compensate for schizophrenia-related medial frontal dysfunction. Molecular psychiatry, 22(5), 647-655.

Perreault, M. L., Hasbi, A., O'dowd, B. F., & George, S. R. (2014). Heteromeric dopamine receptor signaling complexes: emerging neurobiology and disease relevance. Neuropsychopharmacology, 39(1), 156-168.

Perreault, M. L., Fan, T., Banasikowski, T. J., Grace, A. A., & George, S. R. (2017). The atypical dopamine receptor agonist SKF 83959 enhances hippocampal and prefrontal cortical neuronal network activity in a rat model of cognitive dysfunction. European Journal of Neuroscience, 46(4), 2015-2025.

Phillips, A. G., Ahn, S., & Floresco, S. B. (2004). Magnitude of dopamine release in medial prefrontal cortex predicts accuracy of memory on a delayed response task. Journal of Neuroscience, 24(2), 547-553.

R Core Team (2025). R: A Language and Environment for Statistical Computing. Vienna (Austria): R Foundation for Statistical Computing.

Ralph-Williams, R. J., Lehmann-Masten, V., Otero-Corchon, V., Low, M. J., & Geyer, M. A. (2002).

Differential effects of direct and indirect dopamine agonists on prepulse inhibition: a study in D1 and D2 receptor knock-out mice. Journal of Neuroscience, 22(21), 9604-9611.

Robinson, S. E., & Sohal, V. S. (2017). Dopamine D2 receptors modulate pyramidal neurons in mouse medial prefrontal cortex through a stimulatory G-protein pathway. Journal of Neuroscience, 37(42), 10063-10073.

Ruggiero, R. N., Rossignoli, M. T., Lopes-Aguiar, C., Leite, J. P., Bueno-Junior, L. S., & Romcy-Pereira, R. N. (2018). Lithium modulates the muscarinic facilitation of synaptic plasticity and theta-gamma coupling in the hippocampal-prefrontal pathway. Experimental Neurology, 304, 90-101.

Ruggiero, R. N., Rossignoli, M. T., Marques, D. B., de Sousa, B. M., Romcy-Pereira, R. N., Lopes-Aguiar, C., & Leite, J. P. (2021). Neuromodulation of hippocampal-prefrontal cortical synaptic plasticity and functional connectivity: implications for neuropsychiatric disorders. Frontiers in cellular neuroscience, 15.

Schall, K. P., & Dickson, C. T. (2010). Changes in hippocampal excitatory synaptic transmission during cholinergically induced theta and slow oscillation states. Hippocampus, 20(2), 279-292.

Siegle JH, Cuevas López A, Patel YA, Abramov K, Ohayon S, Voigts J (2017) Open Ephys: an open-source, plugin-based platform for multichannel electrophysiology. J Neural Eng 14: 045003

Sigurdsson, T., Stark, K. L., Karayiorgou, M., Gogos, J. A., & Gordon, J. A. (2010). Impaired hippocampal–prefrontal synchrony in a genetic mouse model of schizophrenia. Nature, 464(7289), 763-767.

Sigurdsson, T., & Duvarci, S. (2016). Hippocampal-prefrontal interactions in cognition, behavior and psychiatric disease. Frontiers in systems neuroscience, 9, 190.

Singh, A., Cole, R. C., Espinoza, A. I., Evans, A., Cao, S., Cavanagh, J. F., & Narayanan, N. S. (2021). Timing variability and midfrontal~ 4 Hz rhythms correlate with cognition in Parkinson's disease. npj Parkinson's Disease, 7(1), 14.

Skirboll, L. R., Grace, A. A., & Bunney, B. S. (1979). Dopamine auto-and postsynaptic receptors: electrophysiological evidence for differential sensitivity to dopamine agonists. Science, 206(4414), 80-82.

Spellman, T., Rigotti, M., Ahmari, S. E., Fusi, S., Gogos, J. A., & Gordon, J. A. (2015). Hippocampal–prefrontal input supports spatial encoding in working memory. Nature, 522(7556), 309-314.

Thompson, J. L., Yang, J., Lau, B., Liu, S., Baimel, C., Kerr, L. E., ... & Borgland, S. L. (2016). Age-dependent D1–D2 receptor coactivation in the lateral orbitofrontal cortex potentiates NMDA receptors and facilitates cognitive flexibility. Cerebral Cortex, 26(12), 4524-4539.

Uhlhaas, P. J., Roux, F., Rodriguez, E., Rotarska-Jagiela, A., & Singer, W. (2010). Neural synchrony and the development of cortical networks. Trends in cognitive sciences, 14(2), 72-80.

Vinck, M., Oostenveld, R., Van Wingerden, M., Battaglia, F., & Pennartz, C. M. (2011). An improved index of phase-synchronization for electrophysiological data in the presence of volume-conduction, noise and sample-size bias. Neuroimage, 55(4), 1548-1565.

Weber, M. A., Conlon, M. M., Stutt, H. R., Wendt, L., Ten Eyck, P., & Narayanan, N. S. (2022). Quantifying the inverted U: A meta-analysis of prefrontal dopamine, D1 receptors, and working memory. Behavioral neuroscience, 136(3), 207.

Xu, T. X., & Yao, W. D. (2010). D1 and D2 dopamine receptors in separate circuits cooperate to drive associative long-term potentiation in the prefrontal cortex. Proceedings of the National Academy of Sciences, 107(37), 16366-16371.

Xu, D., Karain, B., Brantley, E., & Shi, W. X. (2011). Effects of L-DOPA on nigral dopamine

661 neurons and local field potential: comparison with apomorphine and muscimol.
662 Journal of Pharmacology and Experimental Therapeutics, 337(2), 533-539.
663 Xu, X., Zheng, C., An, L., Wang, R., & Zhang, T. (2016). Effects of dopamine and serotonin
664
665 systems on modulating neural oscillations in hippocampus-prefrontal cortex pathway
666 in rats. Brain topography, 29(4), 539-551.
667 Yanagihashi, R., Yamanouchi, K., & Ishikawa, T. (1991). The effects of apomorphine on the
668 hippocampal field potential in freely moving rats: pharmacological evidence of the
669 involvement of D2 receptors. Neuropharmacology, 30(2), 177-182.
670 Young-Kim, Y. C., Han, S. W., Alberico, S. L., Ruggiero, R. N., De Corte, B., Chen, K. H., &
671 Narayanan, N. S. (2017). Optogenetic stimulation of frontal D1 neurons compensates
672 for impaired temporal control of action in dopamine-depleted mice. Current biology,
673 27(1), 39-47.
674 Young-Kim, Y. C., & Narayanan, N. S. (2019). Prefrontal D1 dopamine-receptor neurons and
675 delta resonance in interval timing. Cerebral cortex, 29(5), 2051-2060.
676